ACS APPLIED MATERIALS & INTERFACES

Research Article

www.acsami.org

Removal of Cu(II) and Fulvic Acid by Graphene Oxide Nanosheets Decorated with Fe_3O_4 Nanoparticles

Jie Li, Shouwei Zhang, Changlun Chen,* Guixia Zhao, Xin Yang, Jiaxing Li, and Xiangke Wang

Key Laboratory of Novel Thin Film Solar Cells, Institute of Plasma Physics, Chinese Academy of Sciences, P.O. Box 1126, Hefei 230031, P. R. China

Supporting Information

ABSTRACT: Graphene oxide/Fe_3O_4 (GO/Fe_3O_4) composites were synthesized and characterized by scanning electron microscopy, transmission electron microscopy, and X-ray photoelectron spectroscopy. The removal of Cu(II) and a natural organic macromolecule (fulvic acid (FA)) by GO/Fe_3O_4 was investigated. The mutual effects of FA/Cu(II) on Cu(II) and FA sorption onto GO/Fe_3O_4, as well as the effect of pH, ionic strength, FA/Cu(II) concentrations, and the addition sequences of FA/Cu(II) were examined. The results indicated that Cu(II) sorption on GO/Fe_3O_4 were strongly dependent on pH and independent of ionic strength, indicating that the sorption was mainly dominated by inner-sphere surface complexation rather than outer-sphere surface complexation or ion exchange. The presence of FA leads to a strong increase in Cu(II) sorption at low pH and a decrease at high pH, whereas the presence of Cu(II) led to an increase in FA sorption. The adsorbed FA contributes to the modification of sorbent surface properties and partial complexation of Cu(II) with FA adsorbed. Different effects of FA/Cu(II) concentrations and addition sequences on Cu(II) and FA sorption were observed, indicating the difference in sorption mechanisms. After GO/Fe_3O_4 adsorbed FA, the sorption capacity for Cu(II) was enhanced at pH 5.3, and the sorption capacity for FA was also enhanced after Cu(II) sorption on GO/Fe_3O_4. These results are important for estimating and optimizing the removal of metal ions and organic substances by GO/Fe_3O_4 composites.

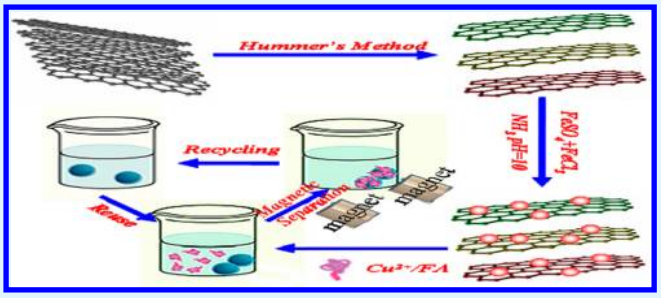

KEYWORDS: *graphene oxide, Fe_3O_4 nanoparticles, sorption, Cu(II), fulvic acid, thermodynamic data*

1. INTRODUCTION

Graphene, a two-dimensional structure of honeycomb carbon lattice, poses as a rising star in material fields due to its large surface area as well as remarkable mechanical, structural, electrical, and thermal properties.[1−11] Graphene oxide (GO) has a wide range of functional groups, such as epoxy, hydroxyl, and carboxyl groups,[12−14] which render it strongly hydrophilic and warrant it a good candidate for the retention and preconcentration of metals, biomolecules, fluorescent molecules, drugs, and inorganic nanoparticles.[15−27] These properties and large specific surface area make GO a superb platform for loading magnetic nanoparticles.[28] The integration of magnetic properties into GO can combine the high sorption capacity of GO and the separation convenience of magnetic materials. Extensive studies have proved that magnetite/graphene nanocomposites exhibit better performances in the removal of contaminants from large volumes of wastewater.[29,30]

In general, organic substances and metal ions exist simultaneously in wastewater, and organic substances can react with metal ions, thereby influencing the removal of metal ions. Therefore, the removal of organic pollutants and heavy metal ions from wastewaters is of considerable practical interest in wastewater treatment, and it is important to study the mutual effect of metal ion and organic substance sorption on graphene composites.

Fulvic acid (FA) is a chemically heterogeneous compound with copious functional groups such as carboxyl, amine, phenol, and hydroxyl. FA has strong complexation ability with metal ions and plays an important role in metal ion speciation in natural waters. FA can react with chlorine during water treatment, thereby producing trihalomethanes, which are carcinogenic. Minimizing FA in drinking water is therefore of considerable practical interest. FA is important for the physicochemical behavior of GO because of the strong interaction of FA with GO through $\pi-\pi$ interactions. FA can interact strongly with GO composites in aquatic systems, thereby greatly enhancing their stability and transport in natural aquatic system. FA may also affect the sorption of some chemical species, mainly metal ions, by forming strong complexes with these metal ions on GO surfaces. Therefore, it is significant to study the sorption behaviors of metal ions on GO composites in the presence of organic substances and vice versa. However, the mutual effect of FA and metal ion sorption

Received: July 17, 2012
Accepted: September 5, 2012
Published: September 5, 2012

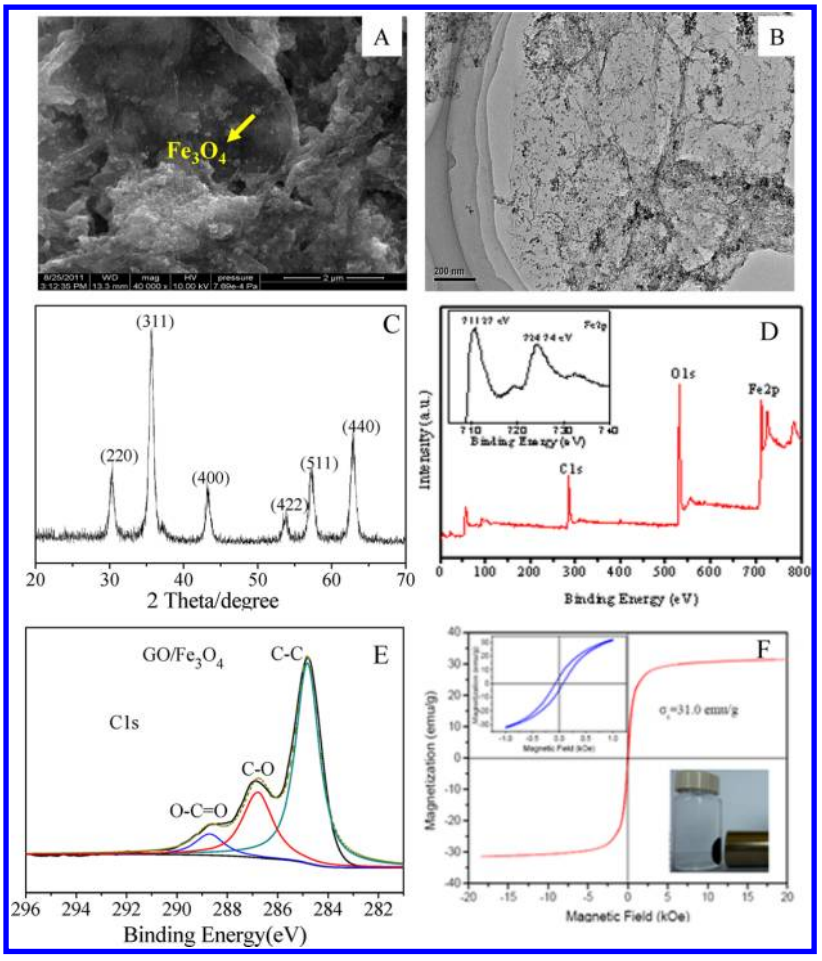

Figure 1. (A) SEM, (B) TEM, (C) XRD pattern, (D) wide scan XPS spectrum of GO/Fe_3O_4 (the inset illustrates the high resolution spectrum of Fe2p peak of GO/Fe_3O_4), (E) high resolution spectrum C 1s peak of GO/Fe_3O_4, and (D) magnetization curve of GO/Fe_3O_4 (below inset being separation of particles of GO/Fe_3O_4 by a magnet).

on GO nanosheets and their composites has not been fully investigated.

In this work, GO/Fe_3O_4 composites were prepared and characterized by scanning electron microscopy (SEM), transmission electron microscopy (TEM), X-ray diffraction (XRD), X-ray photoelectron spectroscopy (XPS), Raman spectroscopy, thermogravimetric analysis−differential thermal analysis (TGA−DTA), and acid−base titration. Batch sorption technique was adopted to evaluate the sorption performance of GO/Fe_3O_4 composites toward Cu(II) and FA as a function of various environmental factors, such as the effect of pH, ionic strength, FA concentrations, and addition sequences of FA/Cu(II). The sorption kinetics and thermodynamics of Cu(II) on GO/Fe_3O_4 composites were analyzed. The reusability of GO/Fe_3O_4 composites was also investigated.

2. EXPERIMENTAL SECTION

2.1. Materials. GO was prepared by using the modified Hummers method[31] from the flake graphite (average particle diameter of 20 mm, 99.95% purity, Qingdao Tianhe Graphite Co. Ltd., China). Briefly, 1.0 g of graphite, 1.0 g of $NaNO_3$, and 40 mL of H_2SO_4 were mixed and stirred in a three neck flask in an acid bath, and then, 6.0 g of $KMnO_4$ was slowly added. Once added, the solution was transferred to a 35 ± 1 °C water bath and stirred for about 1 h; then, 80 mL Milli-Q water was added; and the solution was stirred for 30 min at temperature of 90 ± 1 °C. Then, 150 mL Milli-Q water was added, and 6 mL of H_2O_2 (30%) was added slowly, turning the color of the solution from dark brown to yellow. The warm solution was filtered and rinsed with 100 mL of Milli-Q water. The filter cake was vacuum-dried and a dark brown GO powder was obtained. The typical TEM images, the atomic force microscopy (AFM), and XPS characterization of GO nanosheets are shown in Figure S1, Supporting Information. The TEM and AFM images show that few-layered GO are formed. The GO/Fe_3O_4 was synthesized from GO suspension (0.2 g) in 250 mL solution of 1.86 g $FeCl_3·6H_2O$ and 0.96 g $FeSO_4·7H_2O$ at 80 °C under N_2. The mixed water solution of $FeCl_3$ and $FeSO_4$ was added slowly to the GO suspension, and the ammonia solution was added quickly to precipitate Fe^{2+}/Fe^{3+} ions for synthesis of magnetite (Fe_3O_4) particles. The temperature was raised to 85 °C, and a 30% ammonia solution was added to adjust the pH to 10. After being rapidly stirred for 45 min, the solution was cooled to room temperature. Then, the dark-black colored solution was filtered and washed with Milli-Q water/ethanol and dried in a vacuum at 70 °C. Then, the GO/Fe_3O_4 composites were prepared. Fe_3O_4 was prepared by the same chemical coprecipitation method without GO.

Soil FA was extracted from the soil of HuaJia county (Gansu province, China) and has been characterized in detail.[32,33] All reagents were analytical-grade and were used as received. Milli-Q (Millipore, Billerica, MA) water was used in all experiments.

2.2. Batch Sorption Experiments. Sorption of Cu(II) and/or FA on GO/Fe_3O_4 was carried out by batch sorption technique in a 10 mL polyethylene centrifuge tube, where a stock suspension of the GO/Fe_3O_4 and stock solutions of $NaNO_3$, Cu(II), and/or FA were added to achieve the desired concentrations of the different components. The system was adjusted to the desired pH by adding negligible volumes of 0.01 or 0.1 mol/L NaOH or HNO_3. The suspensions were gently

shaken for 24 h to achieve complete equilibrium. The solid and liquid phases were separated by a magnetic process using a permanent magnet. The concentration of Cu(II) was measured using an atomic absorption spectrophotometer. The concentration of FA in the supernatant was determined on a UV−vis spectrophotometer (UV-2550, Shimadzu, Kyoto, Japan) at 210 nm. The amounts of sorbed Cu(II) or FA were calculated from the difference between the initial concentration (C_0) and equilibrium concentration (C_e) in the supernatant after separation. The sorption percentage [sorption (%) = $(C_0-C_e)/C_0 \times 100$] and distribution coefficient (K_d) [$K_d = (C_0 - C_e)/C_e \times V/m$] were derived from the difference between C_0 and C_e (here, V is the volume of solution, and m is the mass of sorbent).

The effects of FA/Cu concentrations and addition sequences on the sorption of Cu(II) and FA to GO/Fe_3O_4 were also investigated. The addition sequences were expressed as follows: (1) Cu(II) and FA were pre-equilibrated for 24 h before the addition of GO/Fe_3O_4 (described as (Cu(II)-FA)-GO/Fe_3O_4); (2) GO/Fe_3O_4 and Cu(II) were pre-equilibrated for 24 h before the addition of FA (described as (Cu(II)-GO/Fe_3O_4)-FA); (3) GO/Fe_3O_4 and FA were pre-equilibrated for 24 h before the addition of Cu(II) (described as (GO/Fe_3O_4-FA)-Cu(II)).

3. RESULTS AND DISCUSSION

3.1. Characterization of GO/Fe_3O_4. The SEM and TEM images of GO/Fe_3O_4 are shown in Figure 1A and B, and the crumpled silk wave-like graphene sheets and the presence of magnetite nanoparticles suggest that GO/Fe_3O_4 nanocomposites are formed. The TEM image (Figure 1B) shows that the GO film is transparent and Fe_3O_4 nanoparticles are well dispersed on the surface. Closer examination reveals that the average size of the Fe_3O_4 nanoparticles is about 10−15 nm. According to TGA−DTA curves of GO/Fe_3O (Figure S2A, Supporting Information), the weight percent of Fe_3O_4 in GO/Fe_3O_4 is 68.7 wt %.

Figure 1C shows the XRD pattern of GO/Fe_3O_4 structure. The intense diffraction peaks indexed to (220), (311), (400), (422), (511), and (440) planes appearing at 2θ = 30.15°, 36.27°, 43.32°, 53.89°, 57.13°, and 62.29°, respectively, are consistent with the standard XRD data for the cubic phase Fe_3O_4 with a face-centered cubic (fcc) structure (JCPDS No. 89-3854). The broad diffraction peaks are indications of the nanoparticles with very small size.

The chemical state of element in GO/Fe_3O_4 was further investigated by XPS. The wide scan XPS spectrum (Figure 1D) of GO/Fe_3O_4 shows photoelectron lines at binding energies of about 285, 530, and 711 eV, attributed to C1s, O1s, and Fe2p, respectively. In the spectrum of Fe2p (the inset of Figure 1D), the peaks of $Fe2p_{3/2}$ and $Fe2p_{1/2}$ are located at 711.27 and 724.74 eV, not at 710.34 and 724.02 eV, which are for γ-Fe_2O_3.[34] The result is in accordance with the reported data of $Fe2p_{3/2}$ and $Fe2p_{1/2}$, which is indicative of the formation of Fe_3O_4 phase in the composites.[34] Compared to the Fe2p core level XPS spectra of Fe_3O_4 with that of GO/Fe_3O_4, no obvious difference of Fe2p binding energy is found (Figure S2B, Supporting Information). In Figure 1E, the high resolution C1s peak of GO/Fe_3O_4 can be deconvoluted into three components:[35] (1) the nonoxygenated C (284.8 eV); (2) the carbon in C—O (~286.8 eV); and (3) the carboxylate carbon (O—C═O, ~288.8 eV).

The saturation magnetization (Ms) of the GO/Fe_3O_4 composites is 31 emu g^{-1} (magnetic field ±20 kOe) (Figure 1F), indicating the high magnetic property. The inset in Figure 1F is the magnification of hysteresis loop of GO/Fe_3O_4. The inset of Figure 1F shows that GO/Fe_3O_4 is attracted by a magnet, and the clear solution can be easily removed by pipet or decanted. According to the preliminary investigation, the behavior of GO/Fe_3O_4 loaded with FA, Cu(II), or Cu(II)/FA in a magnetic field under neutral, basic, acid conditions has no obvious differences (Figure S3, Supporting Information). This simple magnetic separation experimental result confirms that GO/Fe_3O_4 is magnetic and can be used as a magnetic sorbent to enrich pollutants from large volumes of aqueous solutions.

The surface of sorbent contains a large number of binding sites. Assuming that surface sites (═SOH) are amphoteric, they may become positively charged at low pH due to the protonation reaction on the surfaces (i.e., SOH + $H^+ \Leftrightarrow SOH_2^+$). At high pH values, the surface of adsorbent surfaces becomes negatively charged due to the deprotonation process (i.e., SOH ⇔ $SO^- + H^+$). Surface site density can be estimated from acid−base titration (described in the Supporting Information, SI-4). The acid−base titration data for GO/Fe_3O_4 are shown in Figure 2. TOTH is the total concentration

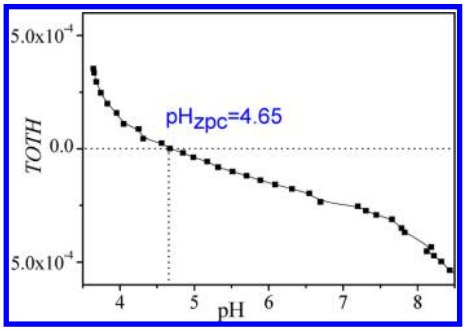

Figure 2. Acid−base titration of GO/Fe_3O_4.

of consumed protons in the titration process, which is calculated from the following equation:

$$\mathrm{TOTH} = \frac{-(V_b - V_{eb1})C_b}{V_0 + V_b} \quad (1)$$

where V_0 represents the initial volume of the suspension, V_b is the total volume of OH^- added at the different titration points, V_{eb1} is the volume of NaOH added in the titration of Gran point to zero at the acidic side, and C_b is the concentration of NaOH. The titration curves collected for in 0.01 M $NaNO_3$ solution display nearly identical buffering capacities across the pH range studied. At pH < 4.3, the surfaces of GO/Fe_3O_4 are positively charged, and at pH > 4.3, the surfaces of GO/Fe_3O_4 are negatively charged. The point of zero change (pH_{pzc}) of GO/Fe_3O_4 is 4.65.

3.2. Effect of Contact Time. The sorption of Cu(II) and FA from aqueous solution on GO/Fe_3O_4 as a function of contact time are shown in Figure 3A and B. The sorption of Cu(II) and FA on GO/Fe_3O_4 increase rapidly during the first 5 and 16 h, then remains constant with increasing contact time. According to these results, 24 h was selected as the shaking time to ensure the full equilibrium in the following experiments.

The kinetic sorption data were simulated with a pseudo-first-order model and a pseudo-second-order model, respectively. The pseudo-second-order equation is generally expressed as

$$\frac{t}{q_t} = \frac{1}{K' q_e^2} + \frac{t}{q_e} \quad (2)$$

where K' (g /(mg h)) is the pseudo-second-order rate constant of sorption, q_t (mg/g) is the amount of Cu(II) and FA adsorbed on GO/Fe_3O_4 at time t (h), and q_e (mg/g) is the

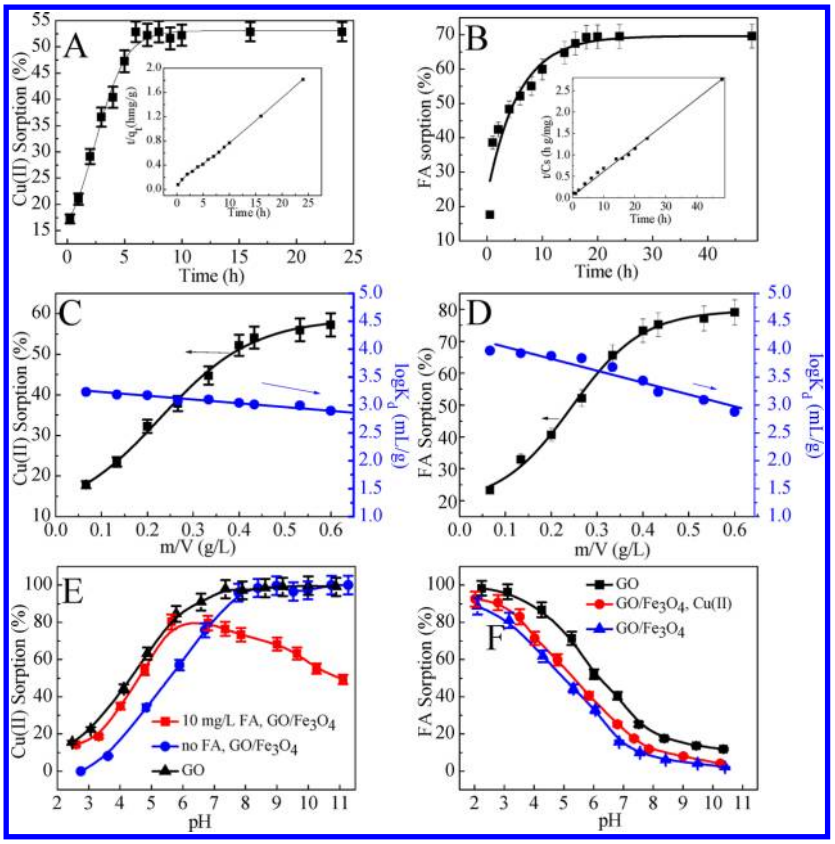

Figure 3. (A) Time-dependent Cu(II) sorption on GO/Fe_3O_4, at pH = 5.3 ± 0.1, $C_{Cu(II)\ initial}$ = 10.0 mg/L, m/V = 0.4 g/L, I = 0.01 M $NaNO_3$, and T = 293 K. (B) Time-dependent FA adsorption on GO/Fe_3O_4, at pH = 5.0 ± 0.1, $C_{FA\ initial}$ = 10.0 mg/L, m/V = 0.4 g/L, I = 0.01 M $NaNO_3$, and T = 293 K. (C) Effect of sorbent content on Cu(II) sorption to GO/Fe_3O_4, at pH = 5.3 ± 0.1, $C_{Cu(II)\ initial}$ = 10.0 mg/L, I = 0.01 M $NaNO_3$, and T = 293 K. (D) Effect of sorbent content on FA adsorption to GO/Fe_3O_4, at pH = 5.0 ± 0.1, $C_{FA\ initial}$ = 10.0 mg/L, I = 0.01 M $NaNO_3$, and T = 293 K. (E and F) Effect of pH on Cu(II) (E) and FA (F) sorption to GO/Fe_3O_4 and GO, $C_{Cu(II)\ initial}$ = 10.0 mg/L, $C_{FA(II)\ initial}$ = 10.0 mg/L, m/V = 0.4 g/L, I = 0.01 M $NaNO_3$, and T = 293 K.

equilibrium sorption capacity. A linear plot feature of q_t versus t is achieved and inserted in Figure 3A and B. The results are listed in Table 1. The pseudo-second-order model fits the experimental data better than pseudo-first-order model (shown in Figure S4, Supporting Information).

Table 1. Constants for the Kinetic Sorption Data Using Different Sorption Models

models	pseudo-first-order		pseudo-second-order	
Cu(II)	q_e (mg/g)	11.339	q_e (mg/g)	14.104
	K (h^{-1})	0.370	K' (g /(mg h))	0.065
	R^2	0.964	R^2	0.999
FA	q_e (mg/g)	9.3354	q_e (mg/g)	18.182
	K (h^{-1})	0.117	K' (g /(mg h))	0.003
	R^2	0.953	R^2	0.996

3.3. Effect of Solid Content. The influence of sorbent content on the sorption of Cu(II) and FA onto GO/Fe_3O_4 (shown in Figure 3C and D) is also investigated. As expected, the sorption of Cu(II) and FA increases obviously with increasing sorbent content. The distribution coefficient (K_d) is independent of sorbent content within the experimental uncertainty. This phenomenon is consistent with the physicochemical properties of K_d values.[36] The particles of GO/Fe_3O_4 are almost not aggregated in the suspension. The Cu(II) ions in solution can freely form complexes at the surfaces of GO/Fe_3O_4, which is not affected by the content of GO/Fe_3O_4.

3.4. Effect of pH. Figure 3E shows that the initial pH value of the aqueous solution plays an important role in the sorption of Cu(II) on GO and GO/Fe_3O_4 in the absence and presence of FA. The sorption of Cu(II) on GO/Fe_3O_4 increases gradually as pH increases from 2.5 to 8.0 and finally maintains the high level with increasing pH. In the case of Cu(II) sorption on GO, the sorption increases from 17% to 85% as pH increases from 2.3 to 7.0. About 99% of initial Cu(II) is sorbed on GO/Fe_3O_4 and GO at pH > 8.0. Similar results were also reported for Cu(II) sorption on bentonite−polyacrylamide composites[37] and multiwalled carbon nanotubes.[38]

Cu(II) species can be present in aqueous solution in the forms of Cu^{2+}, $Cu(OH)^+$, $Cu(OH)_2$, $Cu(OH)_3^-$, and $Cu(OH)_4$[39] (Figure S4, Supporting Information). At pH < 8, the predominant Cu(II) species is Cu^{2+} and the removal of Cu(II) is mainly accomplished by sorption reaction. At pH < pH_{zpc} (~4.5), the surfaces of GO/Fe_3O_4 are positively charged due to protonation reaction. The electrostatic repulsion between positively charged Cu(II) species (Cu^{2+} and $Cu(OH)^+$) and GO/Fe_3O_4 leads to the low sorption of Cu(II) in this pH range. However, at pH > pH_{zpc}, the concentration of deprotonated sites (≡SO^-) increases with increasing pH because of the surface deprotonation reaction. The deprotonated sites (≡SO^-) are more available to retain the metal ions, and surface complexation among Cu^{2+}, $Cu(OH)^+$, and GO/

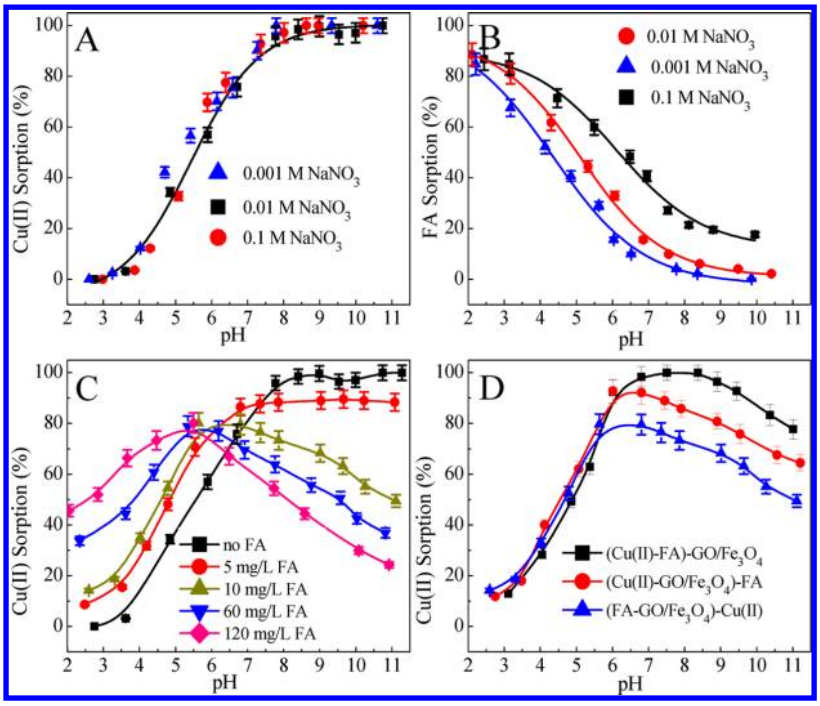

Figure 4. Effect of ionic strength on Cu(II) (A) and FA (B) sorption onto GO/Fe_3O_4, $C_{Cu(II)\ initial}$ = 10.0 mg/L, $C_{FA(II)\ initial}$ = 10.0 mg/L, m/V = 0.4 g/L, and T = 293 K; Effect of FA concentrations on Cu(II) sorption to GO/Fe_3O_4, $C_{Cu(II)\ initial}$ = 10.0 mg/L, m/V = 0.4 g/L, I = 0.01 M $NaNO_3$, and T = 293 K (C); Effect of addition sequences on Cu(II) sorption to GO/Fe_3O_4, $C_{Cu(II)\ initial}$ = 10.0 mg/L, $C_{FA\ initial}$ = 10.0 mg/L, m/V = 0.4 g/L, I = 0.01 M $NaNO_3$, and T = 293 K (D).

Fe_3O_4 is facilitated, thus resulting in a sharp increase of Cu(II) sorption at pH 4.5−8.0. In the pH range of 8.0−11.0, the removal of Cu(II) reaches maximum and remains constant. The main Cu(II) species are $Cu(OH)^+$, $Cu(OH)_2$, and $Cu(OH)_3^-$, and thus, the removal of Cu(II) is possibly accomplished by simultaneous precipitation of $Cu(OH)_2$ and sorption of $Cu(OH)^+$ and $Cu(OH)_3^-$ on GO/Fe_3O_4.

The sorption of Cu(II) shows drastically different trends in the presence of FA (Figure 3E). At pH < 6, the percentage sorption of Cu(II) on GO/Fe_3O_4 is improved, and the maximum sorption lowered by two units (i.e., it shifts from 8.0 to 6.0) than that for the sorption of Cu(II) on GO/Fe_3O_4 in the absence of FA. However, the presence of FA reduces Cu(II) sorption at pH > 8. Yang and Xing[40] determined the ζ-potentials of FA as a function of pH and found that FA has negative zeta potentials at pH > 2. At low pH values, the negatively charged FA can be easily adsorbed on the positively charged GO/Fe_3O_4, so the strong complexation ability of surface-adsorbed FA and Cu(II) results in the improvement of Cu(II) sorption on GO/Fe_3O_4. At high pH values, more free FA molecules remain in the solution, which can form strong FA/Cu(II) complexes and thereby competitively diminish the extent of Cu(II) sorption.[41,42] The fact that fewer FA molecules are adsorbed on GO/Fe_3O_4 (i.e., there are more FA molecules in the solution) indicates that there is less complexation of Cu(II) with adsorbed FA on GO/Fe_3O_4. The sorption of Cu(II) therefore decreases with increasing pH in the presence of FA.

Figure 3F shows that the sorption of FA on GO and on GO/Fe_3O_4 decreases with increasing pH. FA adsorbed on an opposite charged surface experiences not only electrostatic attraction to the surface but also electrostatic repulsion within FA itself.[43] The latter effect occurs at high pH values when the ionization of carboxylic groups increases repulsion in a FA segment, leading to an increase in the FA length. Because FA molecules are large, only a fraction of the FA molecules may participate in the formation of complexes with surface sites. The high sorption of FA at low pH can be attributed to a highly "coiled" FA conformation as a result of low charge development;[44] this results in the sorption of a large number of FA molecules because each molecule occupies a smaller area. At high pH, however, FA is more "stretched", as a result of electrostatic repulsion; so, the area occupied by each molecule will be higher. A lower sorption percentage is therefore obtained at high pH values. At very low pH values, GO would be protonated and become more positively charged; FA molecules are still negatively charged, and so, GO and FA can interact via electrostatic attraction, thereby enhancing the sorption intensity. As the pH increases, the weakly acidic FA, which has carboxylic and phenol moieties, becomes more negatively charged. Thus, at higher pH values, repulsion between FA and the sorbent surfaces would be stronger, hindering the sorption of FA on GO and on GO/Fe_3O_4. Figure 3F indicates that the presence of Cu(II) enhances FA sorption on GO/Fe_3O_4. The interactions between Cu(II) and FA in solution produce a change in the distribution of FA species and therefore influence the extent of sorption. The interactions between Cu(II) and adsorbed FA result in alterations in the packing, spacing, and alignment of adsorbed FA or FA/Cu(II) complexes.[45] The interactions between Cu(II) and GO/Fe_3O_4 neutralize repulsive forces between GO, thus creating favorable sorption sites. Parts E and F of Figure 3 show that the sorption of Cu(II) and FA on GO/Fe_3O_4 surface is lower than that on the GO surface. The loaded Fe_3O_4 particles on the GO surface have few functional groups, thereby decreasing the sorption capacity of GO/Fe_3O_4.

3.5. Effect of Ionic Strength. The sorption of Cu(II) on GO/Fe_3O_4 as a function of pH in 0.1, 0.01, and 0.001 mol/L

$NaNO_3$ solutions are shown in Figure 4A. The effect of the background electrolyte concentrations on Cu(II) sorption to GO/Fe_3O_4 in wide pH range is fairly negligible (Figure 4A). The effect of ionic strength on Cu(II) sorption is consistent with those reported in the literature.[37,38] The background electrolyte concentration affects the thickness and interface potential of the double layer (the surface of GO/Fe_3O_4 and the background solution), which will affect the binding of the adsorbing species.[39] The background electrolyte ions are placed in the same plane as the outer-sphere complexes, consequently, outer-sphere complexes are more impressionable to the variations of ionic strength than inner-sphere complexes. Therefore, the sorption of Cu(II) may be attributed to the formation of inner-sphere complexes on the surfaces of GO/Fe_3O_4. Hayes and Leckie[45] concluded that β-plane sorption can be proposed to occur when the background electrolyte remarkably affects the sorption process; otherwise, o-plane sorption may proceed. The result of this work implies that Cu(II) participates in an o-plane complex reaction, without being affected by the β-plane complex reaction of the background electrolyte (i.e., Na^+ and NO_3^-). The pH-dependent and ionic strength-independent sorption indicate that an inner-sphere surface complexation rather than an ion exchange or an outer-sphere surface complexation contributes to the sorption of Cu(II) on GO/Fe_3O_4.

Sorption of FA on GO/Fe_3O_4 influenced by the ionic strength is shown in Figure 4B. The coiling of FA molecules would increase with the increase of ionic strength, and the structures would become more compact at higher ionic strength.[42] When the FA molecules become more compact, more FA molecules are adsorbed because they occupy a smaller area.

3.6. Effect of FA Concentration. The sorption of Cu(II) on GO/Fe_3O_4 as a function of FA concentration is shown in Figure 4C. FA concentration significantly affects Cu(II) sorption, and different FA concentrations show tremendously different trends. For four FA concentrations studied, Cu(II) sorption on GO/Fe_3O_4 is improved at pH < 5.5 but reveals different trend at pH > 5.5. Concretely, at FA concentration 5 mg/L, the sorption of Cu(II) on GO/Fe_3O_4 has a similar trend compared to Cu(II) sorption in the absence of FA, but the maximum sorption decreases, and the pH at which the Cu(II) sorption reached its maximum value decreased by one pH unit (from 8 to 7) compared to Cu(II) sorption in the absence of FA. At FA concentrations of 10, 60, and 120 mg/L, the higher the FA concentration, the higher the amount of Cu(II) that is sorbed on GO/Fe_3O_4 at pH < 5.5. Whereas, at pH > 5.5, the higher the FA concentration, the lower the amount of Cu(II) that is sorbed on GO/Fe_3O_4. Similar effects of humic substances on the sorption of Pb(II) on to the multiwalled carbon nanotubes/polyacrylamide composites were observed.[41] One interpretation for this different phenomenon may be that, at higher FA concentration, more adsorbed FA on sorbent surface could provide more functional groups, such as carboxylic groups, to form FA/Cu complexes on the sorbent surface at pH < 5.5. Consequently, the maximum sorption amount of Cu(II) shifts to lower pH at higher FA concentration. Whereas, at pH > 5.5, more free FA molecules are available in the solution at higher FA concentration. The free FA molecules can form strong complexes with Cu(II)[42] in the solution, thus fastening Cu(II) in the solution. More FA in the solution implies that there are fewer FA/Cu complexes on the surface of GO/Fe_3O_4, which contributes to the sorption of Cu(II) decreases with increasing pH in the presence of FA, especially at high FA concentrations.

3.7. Effect of Addition Sequences. Figure 4D shows the sorption of Cu(II) for the three different addition sequences. At 10 mg/L FA, I = 0.01 mol/L $NaNO_3$, and an initial Cu(II) concentration of 10 mg/L, the addition sequences have no influence on Cu(II) sorption below pH 5.5. However, differences are observed in the three different addition sequences above pH 6. The observed differences suggest some significant differences in the Cu(II) sorption mechanism on GO/Fe_3O_4. In the case of (GO/Fe_3O_4-Cu(II))-FA, where FA is added to a suspension of GO/Fe_3O_4-Cu(II), complexation between sorbed Cu(II) and the higher molecular weight fraction of FA in solution appears to be less probable, and only a small amount of the free Cu(II) ions in the solution form complexes with FA and then are sorbed on GO/Fe_3O_4. FA consists of heterogeneous components with a wide range of molecular weights and different chemical moieties. As a result of FA component heterogeneities, there may be a broad distribution of sorption affinities for sorbent surfaces. A number of previous reports have shown that the sorption of lower molecular weight FA fractions with more acidic functional groups is higher than that of higher molecular weight fractions.[40] In the case of (GO/Fe_3O_4-FA)-Cu(II), FA adsorbed on GO/Fe_3O_4 mainly consists of lower molecular weight FA fractions; the higher molecular weight FA fractions are thus in suspension. Soluble FA is a higher molecular weight FA fraction than the adsorbed FA. When Cu(II) is added to this suspension, strong complexation with the higher molecular weight FA fractions will stabilize Cu(II) in solution. We speculate that in the (Cu(II)-FA)-GO/Fe_3O_4 system, where Cu(II) is pre-equilibrated with FA, all the Cu(II) ions form complexes with FA and then are sorbed on GO/Fe_3O_4. The complexes probably have different sorption mechanisms for metal ions. It is also possible that a portion of the Cu(II) will be sorbed on the exposed GO/Fe_3O_4 surfaces in complex samples. Hence, in this system, FA/Cu(II) complexes control Cu(II) sorption behavior.

Figure 5 shows that FA adsorption was also dependent on the Cu(II) concentration for all three FA/Cu(II) addition sequences. FA adsorption first increases and then remains at a high level with increasing Cu(II) concentration. According to the analysis of the effect of Cu(II) on FA adsorption, increasing Cu(II) concentrations produce increasingly strong effects on the packing, spacing, or alignment of adsorbed FA, until FA adsorption reaches a maximum. The different FA/Cu(II)

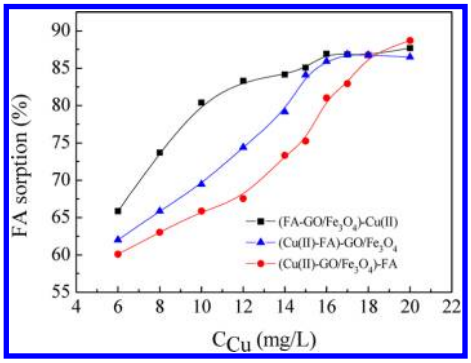

Figure 5. Effects Cu(II) concentration for all three FA/Cu(II) addition sequences on FA adsorption to GO/Fe_3O_4, $C_{FA\ initial}$ = 10.0 mg/L, m/V = 0.4 g/L, I = 0.01 M $NaNO_3$, and T = 293 K.

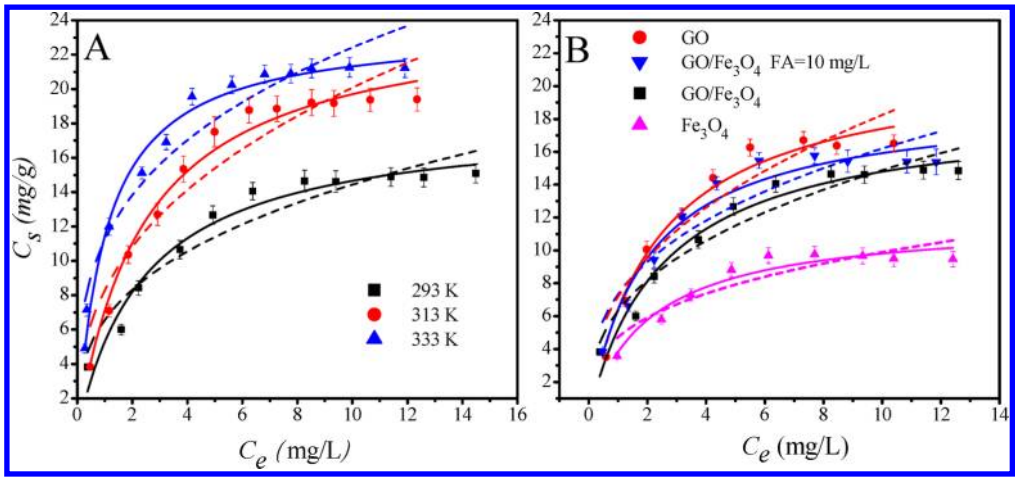

Figure 6. (A) Sorption isotherms of Cu(II) on GO/Fe_3O_4 at three different temperatures. (B) Sorption isotherms of Cu(II) on GO, GO/Fe_3O_4 in the absence and presence of FA and Fe_3O_4 (magnetite nanoparticles prepared by chemical coprecipitation method), at pH = 5.3 ± 0.1, m/V = 0.4 g/L, I = 0.01 M $NaNO_3$, and T = 293 K. Symbols represent experiment data, solid lines represent Langmuir model fitting, and dashed lines represent Freundlich model fitting.

Table 2. Parameters for Langmuir and Freundlich Isotherm Models

	Langmuir model			Freundlich model		
	$C_{s,max}$ (mg/g)	b (L/mg)	R^2	K_F ((mg^{1-n} L^n)/g)	n	R^2
GO/Fe_3O_4, 293 K	18.26	0.942	0.986	6.531	0.417	0.924
GO/Fe_3O_4, 313 K	23.23	0.406	0.986	7.977	0.347	0.934
GO/Fe_3O_4, 333 K	25.57	0.382	0.985	11.254	0.306	0.933
GO, 293 K	21.49	0.502	0.977	7.329	0.314	0.907
GO/Fe_3O_4, FA, 293 K	19.09	0.471	0.963	7.021	0.321	0.906
Fe_3O_4, 293 K	11.89	0.425	0.943	7.201	0.403	0.904

addition sequences also have an important effect on FA adsorption. The observed differences suggest some significant differences in the mechanisms of FA adsorption on GO/Fe_3O_4. In the (GO/Fe_3O_4−Cu(II))-FA system, Cu(II) is pre-equilibrated with GO/Fe_3O_4, and more Cu(II) ions are adsorbed on GO/Fe_3O_4 than in the ternary (GO/Fe_3O_4-FA)-Cu(II) or (Cu(II)-FA)-GO/Fe_3O_4 systems. From the results of Cu(II) and FA adsorption on the systems formed via the three different addition sequences, we can conclude that Cu(II) adsorption on FA-GO/Fe_3O_4 hybrids is governed by both soluble FA in the solution and surface-adsorbed FA.

3.8. Cu(II) Sorption Isotherms. The sorption isotherms obtained at 293, 313, and 333 K are shown in Figure 6A. The Langmuir and Freundlich models were used to simulate the experimental data. The Langmuir isotherm model was used to describe the monolayer sorption process. Its form can be described as the following equation:[46]

$$C_s = \frac{bC_{s,max}C_e}{1 + bC_e} \quad (3)$$

where $C_{s,max}$ (mg/g), the maximum sorption capacity, is the amount of Co(II) at complete monolayer coverage, and b (L/mg) is the constant that relates to the heat of sorption.

The Freundlich isotherm model represents properly the sorption data at low and intermediate concentrations on heterogeneous surfaces. It has the following form:[47]

$$C_s = K_F C_e^n \quad (4)$$

where K_F ((mg^{1-n} L^n)/g) represents the sorption capacity when the equilibrium concentration of metal ions equals to 1, and n represents the degree of dependence of sorption with equilibrium concentration.

The related parameters of the two models are tabulated in Table 2. From the correlation coefficients (R^2) and fitting curves shown in Figure 6A, it is obvious that the Langmuir model fits the experimental data better than the Freundlich model. The fact that the sorption data of Cu(II) is in accordance with the Langmuir model suggests that monolayer coverage of Cu(II) on GO/Fe_3O_4 surfaces is the main sorption mechanism.[48] The values of $C_{s,max}$ calculated from the Langmuir model are the lowest at T = 293 K and the highest at T = 333 K, which indicates that the sorption is improved with increasing temperature.

The thermodynamic parameters ($\Delta G°$, $\Delta S°$, and $\Delta H°$) are calculated from the temperature-dependent sorption isotherms. The free energy change ($\Delta G°$) is derived from the relationship[49]

$$\Delta G° = -RT \ln K° \quad (5)$$

where $K°$ is the sorption equilibrium constant. Values of ln $K°$ are obtained by plotting ln K_d versus C_e and extrapolating C_e to zero. The standard entropy change ($\Delta S°$) is calculated using the following equation:

$$\Delta S° = -\left(\frac{\partial \Delta G°}{\partial T}\right)_P \quad (6)$$

The average standard enthalpy change ($\Delta H°$) is then calculated from the relationship

$$\Delta H° = \Delta G° + T\Delta S° \quad (7)$$

where R (8.314 J/(mol K)) is the ideal gas constant and T (K) is the temperature in Kelvin. The thermodynamic data calculated by eqs 5−7 are tabulated in Table 3. The positive

Table 3. Values of Thermodynamic Parameters for Cu(II) Sorption on GO/Fe_3O_4

	$\Delta G°$ (kJ/mol)	$\Delta S°$ (J/(mol K))	$\Delta H°$ (kJ/mol)
293 K	−21.366	125	15.259
313 K	−23.095		16.030
333 K	−26.398		15.227

$\Delta H°$ values suggest that the sorption is endothermic, which is in accordance with the increasing sorption as the temperature increases. One interpretation for the endothermic phenomenon may be that Cu(II) is dissolved well in water and the hydration sheath of Cu(II) has to be broken down before its sorption on GO/Fe_3O_4. This dehydration process needs energy, and high temperature is beneficial for sorption. This energy exceeds the exothermicity of cations to attach to the solid surface. The assumption indicates that the endothermicity of the desolvation process is higher than the enthalpy of sorption to a considerable extent. The negative $\Delta G°$ values are indicative of a spontaneous process. The value of $\Delta G°$ becomes more negative with the increase of temperature, which indicates more efficient sorption at higher temperature. At high temperature, cations are readily desolvated, and hence, their sorption becomes more favorable. The positive standard entropy change ($\Delta S°$) indicates the fact that the degree of freedom increases at the solid−liquid interface during the sorption of Cu(II) on GO/Fe_3O_4 and also implies some structural changes in GO/Fe_3O_4 during sorption process. Before the sorption occurs, the Cu(II) ions in solution is surrounded by a tightly bound hydration layer where water molecules are more highly ordered than in bulk water. Once Cu(II) ions come into close interaction with the hydration surface of GO/Fe_3O_4, the ordered water molecules in these two hydration layers are compelled and disturbed, resulting in the increased freedom of the system. However, the sorption of Cu(II) ions on GO/Fe_3O_4 may decrease the degree of freedom of system, but the entropy increase of water molecules exceeds the entropy decrease of Cu(II) ions. Above all, it can be concluded that the sorption of Cu(II) on GO/Fe_3O_4 is an endothermic and spontaneous process. However, Wong et al.[50] investigated the sorption of Cu(II) on tartaric acid modified rice husk and found that the sorption was an exothermic and spontaneous process. The results obtained from this work and the above-mentioned references imply that the thermodynamic parameters are related not only to the properties of sorbate but also to the properties of solid particles.[51]

To compare the sorption capacity of different sorbent, the sorption isotherms of Cu(II) on GO/Fe_3O_4 before and after sorption of FA were studied. The Langmuir and Freundlich models were also applied to simulate Cu(II) sorption isotherms. The results indicate that the Langmuir model fits the Cu(II) sorption isotherms very well (Figure 6B). From the Langmuir model, we can obtain the maximum sorption capacity. At pH = 5.3 ± 0.1, the maximum sorption capacities ($C_{s,max}$) of Cu(II) are 18.26 mg/g for GO/Fe_3O_4 without FA and 19.09 mg/g for the (GO/Fe_3O_4-FA)-Cu(II) system. The $C_{s,max}$ values of Cu(II) are 21.49 mg/g for GO and 11.89 mg/g for Fe_3O_4. These results indicate that after GO/Fe_3O_4 adsorbs FA, the sorption capacity for Cu(II) is improved at pH = 5.3 ± 0.1; however, after the Fe_3O_4 particles loaded on the GO surface, the sorption capacity for Cu(II) is reduced. Admitting that the sorption capacity of Cu(II) on GO/Fe_3O_4 is lower than GO, the introduction of magnetic properties into GO provides the separation convenience.

3.9. Comparison of Cu(II) Sorption Capacity with Other Sorbents and Reusability. To evaluate the potential improvements to Cu(II) removal offered by GO/Fe_3O_4 over other sorbents, $C_{s,max}$, a Langmuir parameter that has been used in most of the earlier investigations for defining Cu(II) sorption capacity of different materials was employed in the present study for comparing the efficacy of GO/Fe_3O_4 with those of other sorbents reported in the literature (see Table 4).

Table 4. Comparison of Cu(II) Sorption Capacities of with Other Sorbents

sorbents	solution chemistry conditions	$C_{s,max}$ (mg/g)	refs
palm shell activated carbon	pH = 5.0, T = 300 K	1.26	52
multiwalled carbon nanotubes	pH = 5.9, T = 293 K	3.31	38
pomace ash	pH = 3.0, T = 296 K	6.98	53
bentonite−polyacrylamide	pH = 5.0, T = 300 K	9.36	46
spent activated clay	pH = 5.0, T = 300 K	10.9	54
prawn shell	pH = 6.0, T = 298 K	17.2	55
GO/Fe_3O_4	pH = 5.3, T = 293 K	18.26	this study

Although a direct comparison of GO/Fe_3O_4 with other sorbents is difficult due to the different experimental conditions applied, it has been found that Cu(II) sorption capacity of GO/Fe_3O_4 is higher than that of MWCNTs, bentonite-polyacrylamide, spent activated clay, etc. Moreover, the magnetic separation convenience make GO/Fe_3O_4 an attractive sorbent for the disposal of Cu-bearing wastewater.

The recycling of GO/Fe_3O_4 in the removal of Cu(II) was investigated. After adsorption, desorption was carried out by washing out GO/Fe_3O_4 bound Cu(II) with HNO_3 (pH ∼ 2) and by rinsing GO/Fe_3O_4 with Milli-Q water; then, GO/Fe_3O_4 was dried at 95 °C and reused. From Figure 7, it is observed that the adsorption capacity of Cu(II) decreases slightly from 18.26 mg/g to 17.57 mg/g with increasing times of the reuse, and the decline in efficiency is not more than 5% after recycle for five times, indicating that GO/Fe_3O_4 has a good reusability.

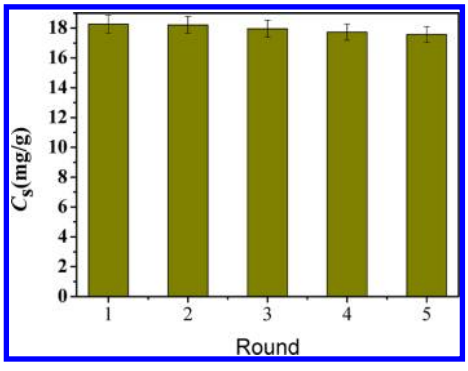

Figure 7. Recycling of GO/Fe_3O_4 in the removal of Cu(II), at pH = 5.3 ± 0.1, I = 0.01 M $NaNO_3$, m/V = 0.4 g/L, and T = 293 K.

The repeated availability is an important factor for an advanced sorbent.

4. CONCLUSIONS

In this study, GO/Fe_3O_4 has been prepared to effectively remove Cu(II) and FA from aqueous solution. The results in this study significantly modify the sorption of metal ions and humic substances in aqueous solution. This research indicates that GO/Fe_3O_4 can be used as an effective sorbent for the simple and rapid removal of inorganic and organic pollutants from water samples.

■ ASSOCIATED CONTENT

Supporting Information

Detailed description for characterization of GO nanosheets, characterization of GO/Fe_3O_4, behavior of GO/Fe_3O_4 loaded with sorbate in magnetic field, the surface charge properties of GO/Fe_3O_4, distribution of Cu(II) species as a function of pH. This information is available free of charge via the Internet at http://pubs.acs.org.

■ AUTHOR INFORMATION

Corresponding Author

*Tel.: +86-551-55933088. Fax: +86-551-5591310. E-mail: clchen@ipp.ac.cn.

Notes

The authors declare no competing financial interest.

■ ACKNOWLEDGMENTS

Financial support from the 973 project of MOST (2011CB933700), the National Natural Science Foundation of China (91126020, 21107115, 21071147, and 21077107), and Natural Science Foundation of Anhui Province (Grant No. 1208085QB32) are acknowledged.

■ REFERENCES

(1) Geim, A. K.; Novoselov, K. S. *Nat. Mater.* **2007**, *6*, 183−191.
(2) Geim, A. K. *Science* **2009**, *324*, 1530−1534.
(3) Zhao, G. X.; Jiang, L.; He, Y. D.; Li, J. X.; Dong, H. K.; Wang, X. K.; Hu, W. P. *Adv. Mater.* **2011**, *23*, 3959−3963.
(4) Avouris, P.; Chen, Z. H.; Perebeinos, V. *Nat. Nanotechnol.* **2007**, *2*, 605−615.
(5) Zhao, G. X.; Li, J. X.; Ren, X. M.; Chen, C. L.; Wang, X. K. *Environ. Sci. Technol.* **2011**, *45*, 10454−10462.
(6) Booth, T. J.; Blake, P.; Nair, R. R.; Jiang, D.; Hill, E. W.; Bangert, U.; Bleloch, A.; Gass, M.; Novoselov, K. S.; Katsnelson, M. I.; Geim, A. K. *Nano Lett.* **2008**, *8*, 2442−2446.
(7) Zhao, G. X.; Ren, X. M.; Gao, X.; Tan, X. L.; Li, J. X.; Chen, C. L.; Huang, Y. Y.; Wang, X. K. *Dalton Trans.* **2011**, *40*, 10945−40952.
(8) Park, S. Y.; Park, J.; Sim, S. H.; Sung, M. G.; Kim, K. S.; Hong, B. H.; Hong, S. *Adv. Mater.* **2011**, *23*, H263−H267.
(9) Lee, W. H.; Park, J.; Sim, S. H.; Lim, S.; Kim, K. S.; Hong, B. H.; Cho, K. *J. Am. Chem. Soc.* **2011**, *133*, 4447−4454.
(10) Lee, J. Y.; Hong, B. H.; Kim, W. Y.; Min, S. K.; Kim, Y.; Jouravlev, M. V.; Bose, R.; Kim, K. S.; Hwang, I.; Kaufman, L. J.; Wong, C. W.; Kim, P.; Kim, K. S. *Nature* **2009**, *460*, 498−501.
(11) Bae, S. K.; Kim, H.; Lee, Y. B.; Xu, X. F.; Park, J. S.; Zheng, Y.; Balakrishnan, J.; Lei, T.; Kim, H. R.; Song, Y.; Il Kim, Y. J.; Kim, K. S.; Özyilmaz, B.; Ahn, J. H.; Hong, B. H.; S, I.. *Nat. Nanotech.* **2010**, *5*, 574−578.
(12) Nakada, K.; Fujita, M.; Dresselhaus, G. *Phys. Rev. B* **1996**, *54*, 17954−17961.
(13) He, H.; Klinowski, J.; Forster, M. *Chem. Phys. Lett.* **1998**, *287*, 53−56.
(14) Lerf, A.; He, H.; Forster, M.; Klinowski, J. *J. Phys. Chem. B* **1998**, *102*, 4477−4482.
(15) Scheuermann, G. M.; Rumi, L.; Steurer, P.; Bannwarth, W.; Mulhaupt, R. J. J. *Am. Chem. Soc.* **2009**, *131*, 8262−8270.
(16) Goncalves, G.; Marques, P.; Granadeiro, C. M.; Nogueira, H. I. S.; Singh, M. K.; Gracio, J. *Chem. Mater.* **2009**, *21*, 4796−4802.
(17) Xu, C.; Wang, X.; Zhu, J. W. *J. Phys. Chem. C* **2008**, *112*, 19841−19845.
(18) Pasricha, R.; Gupta, S.; Srivastava, A. K. *Small* **2009**, *5*, 2253−2259.
(19) Cao, A.; Liu, Z.; Chu, S.; Wu, M.; Ye, Z.; Cai, Z.; Chang, Y.; Wang, S.; Gong, Q.; Liu, Y. *Adv. Mater.* **2009**, *21*, 103−106.
(20) Lu, A. H.; Salabas, E. L.; Schuth, F. *Angew. Chem., Int. Ed.* **2007**, *46*, 1222−1244.
(21) Frey, N. A.; Peng, S.; Cheng, K.; Sun, S. H. *Chem. Soc. Rev.* **2009**, *38*, 2532−2542.
(22) Lee, W. H.; Suk, J. W.; Chou, H.; Lee, J.; Hao, Y. F.; Wu, Y. P.; Piner, R.; Akinwande, D.; Kim, K. S.; Ruoff, R. S. *Nano Lett.* **2012**, *12*, 2374−2346.
(23) Lee, W. H.; Suk, J. W.; Lee, J.; Hao, Y.; Park, J.; Yang, J. W.; Ha, H. W.; Murali, S.; Chou, H.; Akinwande, D.; Kim, K. S.; Ruoff, R. S. *ACS Nano* **2012**, *6*, 1284−1290.
(24) Huh, S.; Park, J.; Kim, Y. S.; Kim, K. S.; Hong, B. H.; Nam, J. M. *ACS Nano* **2011**, *5*, 9799−9806.
(25) Jeong, W. Y.; Park, J.; Kwang, S.; Kim, B. H. *Org. Biomol. Chem.* **2011**, *9*, 7434−7437.
(26) Myung, S.; Park, J.; Lee, H.; Kim, K. S.; Hong, S. *Adv. Mater.* **2010**, *22*, 2045−2049.
(27) Jabeen, H.; Chandra, V.; Jung, S.; Lee, J. W.; Kim, K. S.; Kim, S. B. *Nanoscale* **2011**, *3*, 3583−3585.
(28) Kassaee, M. Z.; Motamedi, E.; Majdi, M. *Chem. Eng. J.* **2011**, *172*, 540−549.
(29) Chandra, V.; Park, J.; Chun, Y.; Lee, J. W.; Hwang, I. C.; Kim, K. S. *ACS Nano* **2010**, *4*, 3979−3986.
(30) Sreeprasad1, T. S.; Maliyekkal1, S. M.; Lisha, K. P.; Pradeep, T. *J. Hazard. Mater.* **2011**, *186*, 921−931.
(31) Hirata, M.; Gotou, T.; Horiuchi, S.; Fujiwara, M.; Ohba, M. *Carbon* **2004**, *42*, 2929−2937.
(32) Tao, Z. Y.; Zhang, J.; Zhai, J. *Anal. Chim. Acta* **1999**, *395*, 199−203.
(33) Zhang, J.; Zhai, J. J.; Zhao, F. Z.; Tao, Z. Y. *Anal. Chim. Acta* **1999**, *378*, 177−182.
(34) Lu, J.; Jiao, X.; Chen, D.; Li, W. *J. Phys. Chem. C* **2009**, *113*, 4012−4017.
(35) Wang, Y.; Shao, Y. Y.; Matson, D. W.; Li, J. H.; Lin, Y. H. *ACS Nano* **2010**, *4*, 1790−1798.
(36) Yang, S. T.; Li, J. X.; Lu, Y; Chen, Y. X.; Wang, X. K. *Appl. Radiat. Isot.* **2009**, *67*, 1600−1608.
(37) Zhao, G. X.; Zhang, H. X.; Fan, Q. H.; Ren, X. M.; Li, J. X.; Chen, Y. X.; Wang, X. K. *J. Hazard. Mater.* **2010**, *173*, 661−668.
(38) Sheng, G. D.; Li, J. X.; Shao, D. D.; Hu, J.; Chen, C. L.; Chen, Y. X.; Wang, X. K. *J. Hazard. Mater.* **2010**, *178*, 333−340.
(39) Yang, S. T.; Sheng, G. D.; Guo, Z. Q.; Tan, X. L.; Xu, J. Z.; Wang, X. K. *Sci. China Chem.* **2012**, *55*, 632−642.
(40) Yang, K.; Xing, B. S. *Environ. Pollut.* **2009**, *157*, 1095−1100.
(41) Yang, S. B.; Hu, J.; Chen, C. L.; Shao, D. D.; Wang, X. K. *Environ. Sci. Technol.* **2011**, *45*, 3621−3627.
(42) Floroiu, R. M.; Davis, A. P.; Torrents, A. *Environ. Sci. Technol.* **2001**, *35*, 348−353.
(43) Chen, C. L.; Wang, X. K.; Nagatsu, M. *Environ. Sci. Technol.* **2009**, *43*, 2362−2367.
(44) Yoon, T. H.; Moon, H.; Park, Y. J.; Park, K. K. *Environ. Sci. Technol.* **1994**, *28*, 2139−2146.
(45) Hayes, K. F.; Leckie, J. O. *J. Colloid Interface Sci.* **1987**, *115*, 564−572.
(46) Yang, S. T.; Guo, Z. Q.; Sheng, G. D.; Wang, X. K. *Sci. Total Environ.* **2012**, *420*, 214−221.
(47) Yang, S. T.; Li, J. X.; Shao, D. D.; Hu, J.; Wang, X. K. *J. Hazard. Mater.* **2009**, *166*, 109−116.

(48) Zhou, Y. T.; Nie, H. L.; Branford-White, C.; He, Z. Y.; Zhu, L. M. *J. Colloid Interface Sci.* **2009**, *330*, 29−37. Chen, C. L.; Wang, X. K. *Ind. Eng. Chem. Res.* **2006**, *45*, 9144−9149.
(49) Yang, S. T.; Sheng, G. D.; Tan, X. L.; Hu, J.; Du, J. Z.; Montavon, G.; Wang, X. K. *Geochim. Cosmochim. Acta* **2011**, *75*, 6520−6534.
(50) Wong, K. K.; Lee, C. K.; Low, K. S.; Haron, M. J. *Chemosphere* **2003**, *50*, 23−28.
(51) Shao, D. D.; Fan, Q. H.; Li, J. X.; Niu, Z. W.; Wu, W. S.; Chen, Y. X.; Wang, X. K. *Microporous Mesoporous Mater.* **2009**, *123*, 1−9.
(52) Onundi, Y. B.; Mamun, A. A.; Khatib, M. F.; Ahmed, Y. M. *Int. J. Environ. Sci. Tech.* **2010**, *7*, 751−758.
(53) Chu, K. H. *J. Hazard. Mater.* **2002**, *B90*, 77−95.
(54) Weng, C. H.; Tsai, C. Z.; Chu, S. H.; Sharma, Y. C. *Sep. Purif. Technol.* **2007**, *54*, 187−197.
(55) Bouzid, J.; Elouear, Z.; Ksibi, M.; Feki, M.; Montiel, A. *J. Hazard. Mater.* **2008**, *152*, 838−845.